In Situ Fabrication and Reactivation of Highly Selective and Stable Ag Catalysts for Electrochemical CO_2 Conversion

Ma, Ming; Liu, Kai; Shen, Jie; Kas, Recep; Smith, Wilson A.

DOI
10.1021/acsenergylett.8b00472

Publication date
2018

Document Version
Final published version

Published in
ACS Energy Letters

ACS Energy LETTERS

Cite This: ACS Energy Lett. 2018, 3, 1301−1306

LETTER

In Situ Fabrication and Reactivation of Highly Selective and Stable Ag Catalysts for Electrochemical CO_2 Conversion

Ming Ma,*,† Kai Liu,† Jie Shen,‡ Recep Kas,† and Wilson A. Smith*,†

†Materials for Energy Conversion and Storage (MECS), Department of Chemical Engineering, Delft University of Technology, Van der Maasweg 9, 2629 HZ Delft, The Netherlands

‡QuTech and Kavli Institute of Nanoscience, Delft University of Technology, Delft 2600 GA, The Netherlands

Supporting Information

ABSTRACT: In this work, the highly selective and stable electrocatalytic reduction of CO_2 to CO on nanostructured Ag electrocatalysts is presented. The Ag electrocatalysts are synthesized by the electroreduction of Ag_2CO_3 formed by in situ anodic-etching of Ag foil in a $KHCO_3$ electrolyte. After 3 min of this etching treatment, the Ag_2CO_3-derived nanostructured Ag electrocatalysts are capable of producing CO with up to 92% Faradaic efficiency at an overpotential as low as 290 mV, which surpasses all of the reported Ag catalysts at identical conditions to date. In addition, the anodic-etched Ag retained ∼90% catalytic selectivity in the electroreduction of CO_2 to CO for more than 100 h. The Ag_2CO_3-derived Ag is able to facilitate the activation of CO_2 via reduction of the activation energy barrier of the initial electron transfer and provide an increased number of active sites, resulting in the dramatically improved catalytic activity for the reduction of CO_2 to CO.

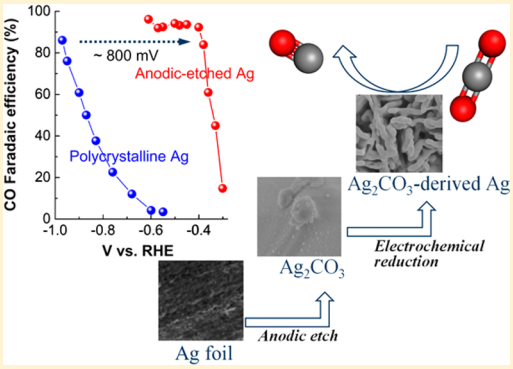

The electrocatalytic conversion of CO_2 into carbon-based fuels and valuable chemicals powered by renewable electricity is an attractive solution to both the utilization of captured CO_2 and the storage of renewable energy.[1−6] An essential step for achieving this goal is to find a highly efficient and selective electrocatalyst with long-term stability.[7,8] Many transition metal catalysts have been evaluated for the selective reduction of CO_2 in CO_2-saturated aqueous solutions.[2,9] Currently, the electrochemical conversion of CO_2 into CO provides one of the most promising routes to form a cost-competitive product because syngas (CO and H_2) can be employed in Fischer−Tropsch synthesis to produce value-added chemicals and synthetic fuels using already existing industrial technologies.[1,4,10] Therefore, significant attention has been focused on finding electrocatalysts that can selectively produce CO from CO_2.[11−18]

While Au is the most active surface for reducing CO_2 selectively to CO among the identified metal catalysts, its potential for industrial applications is currently limited by its low abundance and high cost. In this context, Ag has great potential for large-scale applications due to its significantly lower cost than Au and high catalytic selectivity for the reduction of CO_2 to CO.[9−11,19−24] However, high overpotentials (η) required for driving selective CO_2 reduction and rapid catalytic deactivation in favor of H_2 evolution on Ag catalysts significantly restrict its practical utilization.[20,25]

To overcome the limitations of Ag electrocatalysts, many attempts have focused on the development of nanostructured surfaces, which offer mass-transport advantages and contain more low-coordinated sites (edge sites and corner sites) that are more active for CO_2 reduction in comparison with a planar metallic surface.[7,10,14,22,26,27] It has been demonstrated that nanoporous Ag catalysts prepared by dealloying,[10] Ag nanocoral catalysts synthesized via an oxidation−reduction process using chloride anions[28] and oxide-derived nanostructured Ag[22] are capable of electrochemically reducing CO_2 to CO with dramatically enhanced catalytic selectivity at reduced overpotentials, which are ascribed to fast initial electron transfer for CO_2 activation on these nanostructured catalysts. In addition, the catalytic stability of the electroreduction of CO_2 to CO has been improved on nanostructured Ag catalysts,[10,22,28] owing to the enhanced tolerance to heavy metal impurities in the electrolyte.[27] While these previous attempts have significantly improved the performance of Ag electrocatalysts, it is still critical to develop a very simple, fast, scalable and low-cost method for preparing and maintaining higher-performance Ag

Received: March 23, 2018
Accepted: May 8, 2018
Published: May 8, 2018

DOI: 10.1021/acsenergylett.8b00472
ACS Energy Lett. 2018, 3, 1301−1306

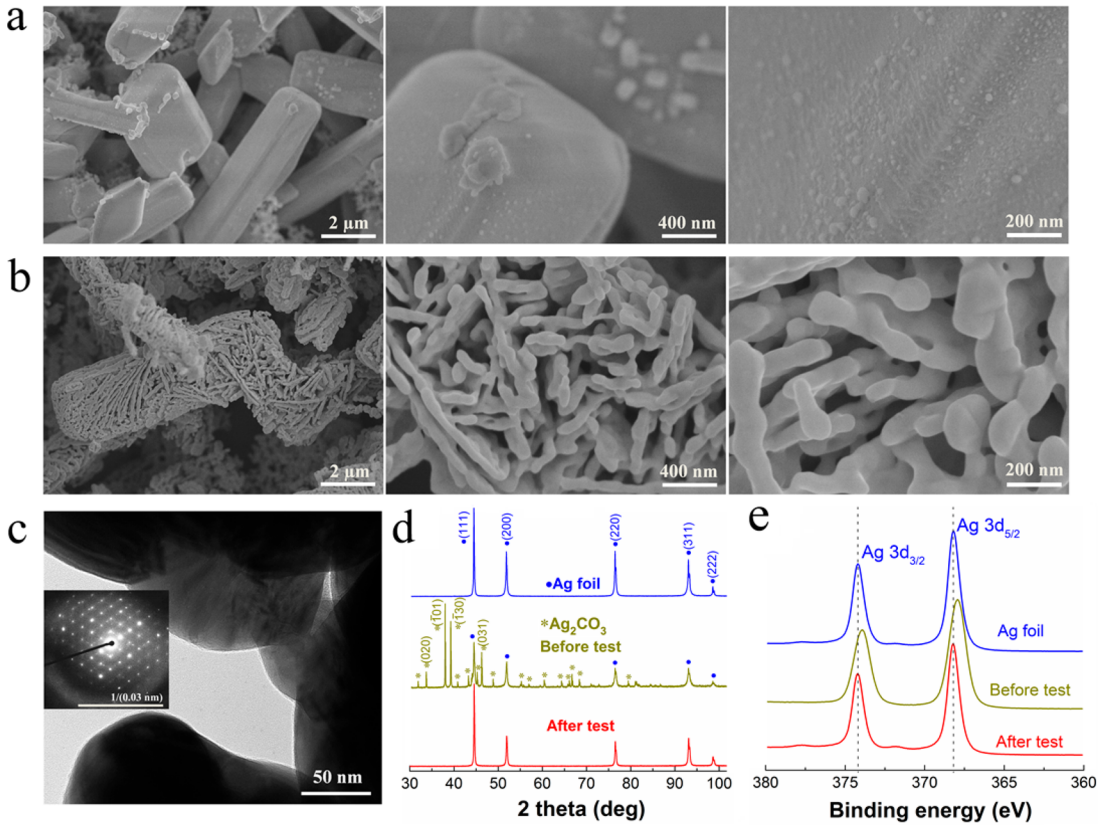

Figure 1. SEM images of anodic-etched Ag (AE-Ag) (4.9 μm) before (a) and after (b) CO_2 reduction electrolysis. (c) TEM image of AE-Ag after CO_2 reduction electrolysis (the inset is the SAED pattern). (d) XRD patterns and (e) XPS spectra of untreated polycrystalline Ag (blue line) and AE-Ag before (dark yellow line) and after (red line) CO_2 reduction electrolysis, respectively.

electrocatalysts for practical applications of CO_2 electroreduction.

Herein, we demonstrate a simple technique to prepare highly active, stable, and selective Ag electrocatalysts in CO_2-saturated $KHCO_3$ electrolyte that is used for CO_2 reduction. By first anodic-etching Ag to form Ag_2CO_3 and then further reducing the Ag_2CO_3 to metallic Ag with a highly porous scaffold structure, a significantly reduced overpotential for high CO catalytic selectivity was achieved with remarkable catalytic stability, which outcompetes the reported Ag catalysts to date at identical conditions. Thus, the robust performance of the nanostructured catalysts formed via this very easy and low-cost synthesis method may offer a platform for practical applications of CO_2 electroreduction.

For the electrochemical synthesis of Ag electrocatalysts used in this work, a polycrystalline Ag foil electrode was immersed in a CO_2-saturated 0.1 M $KHCO_3$ electrolyte in a two-compartment cell using a three-electrode configuration (a Pt counter electrode and a Ag/AgCl reference electrode). The two-compartment cell was separated by a Nafion-115 proton exchange membrane to minimize impurity deposition during electrolysis. An anodic potential of 2.6 V vs the reversible hydrogen electrode (RHE) was applied on the Ag foil electrodes for 3 min to synthesize the Ag_2CO_3 layer, with an estimated thickness of ~4.9 μm (Table S1). The Ag_2CO_3 electrodes were then directly utilized for electrocatalytic CO_2 reduction in CO_2-saturated 0.1 M $KHCO_3$ electrolyte and were electrochemically reduced to metallic Ag in the initial period (<2 min) of CO_2 reduction electrolysis (Figure S5d).

In the initial anodic-etching, the Ag electrodes formed short microporous polyhedral rod-like morphologies with smooth surfaces, as presented in Figure 1a, which is consistent with the reported morphologies of Ag_2CO_3.[29] Figure 1b shows scanning electron microscope (SEM) images of the same electrodes after the electrolysis (~0.5 h) of CO_2 reduction, revealing that a nanoporous structure was formed via the electroreduction of Ag_2CO_3. In addition, transmission electron microscopy (TEM) confirmed that the size of the nanostructured materials after the CO_2 reduction (Figure 1c), and the selected-area electron diffraction (SAED) pattern in the inset of Figure 1c exhibits the typical nature of crystals. To identify the phase of the prepared materials, X-ray diffraction (XRD) measurements were conducted. The XRD diffractograms in Figure 1d indicate that Ag_2CO_3 was formed by anodic-etching of Ag foil in $KHCO_3$ solution. After CO_2 reduction electrolysis, only Ag diffraction peaks were observed (Figure 1d) without any remaining Ag_2CO_3, indicating a full transformation from Ag_2CO_3 to metallic Ag.

To verify the surface composition of our samples, X-ray photoelectron spectroscopy (XPS) measurements were performed. As shown in Figure 1e, the Ag $3d_{5/2}$ peak at 368.2 eV was observed for polycrystalline Ag. For the anodic-etched Ag (AE-Ag) before CO_2 reduction electrolysis, the Ag $3d_{5/2}$ peak shifted by about 0.3 eV to the binding energy of 367.9 eV compared to the metal Ag, which is consistent with the value of Ag^+ in the synthesized Ag_2CO_3 according to previous work.[29−31] In addition, the binding energy of 288.7 eV in C_{1s} spectra (Figure S3) represents the carbon associated with the carbonate ($(CO_3)^{2-}$),[32] which further confirms the formation

DOI: 10.1021/acsenergylett.8b00472
ACS Energy Lett. 2018, 3, 1301−1306

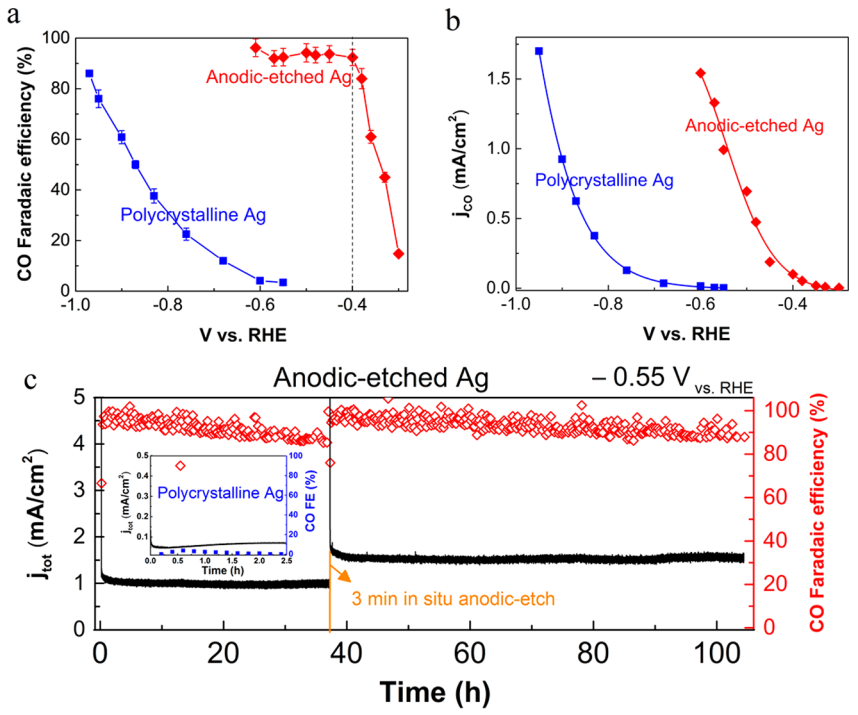

Figure 2. Comparison of the electrocatalytic activity of polycrystalline Ag and AE-Ag (4.9 μm). (a) FE for CO at various potentials in CO_2-saturated 0.1 M $KHCO_3$ (pH 6.8). (b) Current density for CO formation at various potentials. (c) Catalytic stability performance for AE-Ag. The inset shows the catalytic stability of untreated polycrystalline Ag. All of the potentials were *iR*-corrected.

of Ag_2CO_3. After electrolysis, the Ag $3d_{5/2}$ peak shifted back to 368.2 eV, corresponding to metallic Ag[0].[29−31] Furthermore, a surface valence band XPS spectrum of AE-Ag after electrolysis is in line with that of metallic Ag foil (Figure S4). All of the above results indicate that the reduction of Ag_2CO_3 to metallic Ag was complete, implying that only metallic Ag was present on AE-Ag after CO_2 reduction electrolysis.

Figure 2a presents a comparison of the electrocatalytic activity of CO_2 reduction for untreated polycrystalline Ag (in blue) and 4.9 μm AE-Ag (in red) at various applied potentials (*iR*-corrected potentials). Both the AE-Ag and untreated Ag experienced a gradually enhanced Faradaic efficiency (FE) for CO production at more negative potentials (Figure 2a), simultaneously accompanying with a decrease in the related FE for H_2 formation (Figure S6). Notably, the overpotential required for achieving >90% FE for CO production was shifted toward the positive potential by ~800 mV on AE-Ag compared to that of untreated Ag. More importantly, a high FE of more than 92% for CO formation was achieved on AE-Ag at a potential of −0.4 V vs RHE, which corresponds to an overpotential (η_{co}) as low as 0.29 V relative to the CO_2/CO equilibrium potential of −0.11 V vs RHE, representing the highest catalytic selectivity for CO_2 reduction to CO among the reported Ag catalysts at the same η_{co} (Table S2). In contrast, no CO production was detected on untreated polycrystalline Ag at identical conditions (η_{co} = 0.29 V). A plot of the partial current density for CO production (j_{co}) as a function of potential in Figure 2b suggests that the onset potential for the reduction of CO_2 to CO on AE-Ag was −0.3 V vs RHE (η_{co} = 0.19 V), which is a positive shift of ~250 mV in comparison with that (−0.55 V vs RHE) of untreated polycrystalline Ag. These results show that Ag_2CO_3-derived nanostructured Ag is a highly selective electrocatalyst for the electrocatalytic reduction of CO_2 to CO while inhibiting H_2 evolution at significantly reduced overpotentials.

To test the electrocatalytic stability of AE-Ag catalysts, a long-term CO_2 reduction measurement was performed on AE-Ag at a fixed potential of −0.55 V vs RHE ($KHCO_3$ electrolyte without any purification was used). As shown in Figure 2c, AE-Ag exhibited an initially high geometric current density (j_{tot}) at the early stage of electrolysis owing to the electroreduction of Ag_2CO_3 to Ag and subsequently a stable j_{tot} of ~1 mA/cm^2 with a FE of ~90% for CO production over ~37 h. After ~37 h, slight catalytic deactivation for CO formation was found, which may result from the deposition of impurities on the surface of the catalyst during the electrochemical reduction of CO_2.[9,27] To overcome this slight deactivation, the same Ag catalyst electrodes were then held at an anodic potential of 2.6 V vs RHE for 3 min in the same CO_2-saturated $KHCO_3$ electrolyte, and after returning back to −0.55 V vs RHE, a FE as high as ~90% for CO formation was recovered and maintained for more than 60 h (no replacement of electrolyte during >100 h electrolysis). This remarkable stability significantly surpasses the currently reported durability for CO_2 reduction on single-element catalysts (Table S3) under similar conditions. The in situ reactivation of the catalysts may be attributed to the removal of impurities on the surface of the catalysts by anodic-etching the contaminated surface. In contrast, the polycrystalline Ag electrodes had a very low j_{tot} (~0.07 mA/cm^2) and a very low FE for CO, which decreased from 3.4 to 0% over the course of 2.5 h at −0.55 V vs RHE, which indicates fast catalytic deactivation. Thus, the Ag resulting from AE-Ag exhibited high catalytic selectivity and activity with long-term stability for the electrocatalytic reduction of CO_2 to CO.

The electrochemical active surface area (EASA) of nanoporous Ag catalysts reduced from AE-Ag and untreated polycrystalline Ag was measured by forming a monolayer

DOI: 10.1021/acsenergylett.8b00472
ACS Energy Lett. 2018, 3, 1301−1306

oxide on Ag surface in 0.1 M KOH.[20] The charge used for oxidizing the monolayer of the Ag surface was calculated in Figure S7, which shows that the EASA of nanoporous Ag catalysts reduced from AE-Ag (3 min) is more than 10-fold larger than that of untreated Ag, resulting in the discrepancy of j_{tot} between AE-Ag (~1 mA/cm^2) and untreated Ag (~0.07 mA/cm^2), as shown in Figure 2c. Thus, the increased number of active sites (increased EASA) reflects the enhanced catalytic reaction rate. In addition, the normalized j_{co} of AE-Ag by EASA (~0.08 mA/cm^2) is ~40 times higher in comparison with that (~0.002 mA/cm^2) of untreated Ag, indicating significantly improved intrinsic CO_2 reduction activity on nanoporous Ag catalysts reduced from Ag_2CO_3.

The thickness effect of AE-Ag on the catalytic performance was also evaluated. In this work, the average thickness of AE-Ag was tuned by systematically varying the anodic-etching time (Table S1). As shown in Figure 3a, the thickness of AE-Ag is

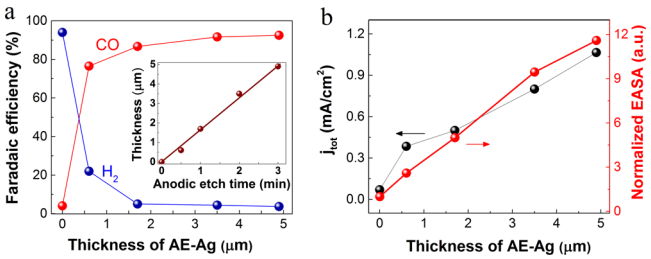

Figure 3. Electrocatalytic activity as a function of the thickness of AE-Ag at −0.55 V vs RHE. (a) FE for CO and H_2 on AE-Ag with different thickness in CO_2-saturated 0.1 M $KHCO_3$ (pH 6.8). The inset shows the thickness for different anodic-etching times. (b) Geometric current density and normalized EASA.

linearly correlated with the anodic-etching time, and an gradually enhanced FE for CO formation was observed along with decreased FE for H_2 evolution at −0.55 V vs RHE with increasing thickness (≤3.5 μm) of AE-Ag. While a high FE of >90% for CO formation was achieved on both 3.5 and 4.9 μm AE-Ag (Figure 3a), the distinct thickness leads to a discrepancy of j_{tot} between the two catalysts (Figure 3b). The EASA was enhanced with increasing thickness of AE-Ag (Figure 3b), which led to the correspondingly increased j_{tot} and j_{co} (Figure S8). These results indicate that the thicker nanoporous Ag is able to provide more active sites for the reduction of CO_2 to CO.

It has been reported that the surface facets of Ag could significantly influence the catalytic activity of CO_2 reduction.[20,33] To reveal the variation of Ag surface facets before and after anodic treatment, the adsorption/desorption of OH^- was performed on AE-Ag and untreated Ag in argon-purged 0.1 M KOH in the potential range from ~−0.3 to ~1 V vs RHE (double layer region) at room temperature.[34−36] Figure 4a exhibits the difference in peak potentials for the OH^- adsorption/desorption processes between AE-Ag (red) and polycrystalline Ag (blue), which correlate with the distinct surface facets of the two catalysts.[34−36] In addition, cyclic voltammetry of oxide-derived Ag reported in our previous work[22] was also conducted in argon-purged 0.1 M KOH, which shows different peak potentials compared to AE-Ag (Figure S11), reflecting different dominant facets of the Ag surface. While the specific facets of the Ag surface could not be identified, the obvious discrepancy in Ag surface facets may contribute to the difference of the catalytic performance in the

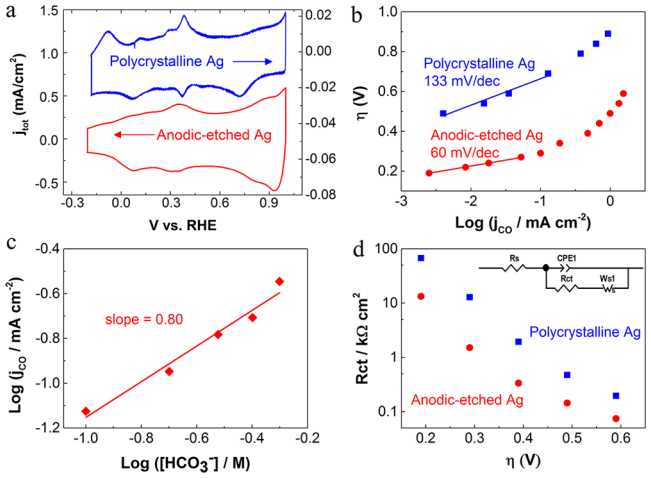

Figure 4. (a) Cyclic voltammetry curves of untreated polycrystalline Ag (blue line) and AE-Ag (4.9 μm) (red line) in argon-purged 0.1 M KOH at room temperature with a sweep rate of 50 mV/s. (b) Tafel plots of the CO partial current density for polycrystalline Ag and AE-Ag (4.9 μm). (c) Bicarbonate concentration at constant potentials of AE-Ag. (d) Charge transfer resistance at various overpotentials. The inset shows the equivalent circuit for the metal/solution interface (R_{ct}, R_s, CPE and W_s are charge transfer resistance, solution resistance, constant phase element, and Warburg-short circuit terminus, respectively).

reduction of CO_2. Therefore, in addition to the increased EASA in the anodic-etched nanostructured Ag compared to polycrystalline Ag, we also provide evidence of a different surface electronic structure that could also influence the catalytic activity and selectivity.

In order to gain insight into the electrokinetic mechanism of CO_2 reduction on AE-Ag and untreated polycrystalline Ag, Tafel analysis was performed. It has been demonstrated that a two-electron transfer is involved for CO_2 reduction to CO, and each electron transfer is followed with one proton donation step (or proton-coupled electron transfer steps based on computational studies[37−40]).[7,9,10,22,27] Of particular note, the initial electron transfer for CO_2 activation (stabilization of $CO_2^{\bullet-}$ or $COOH^{\bullet}$) is the rate-determining step (RDS) in the whole process due to the much higher activation energy barrier for the first electron transfer compared to the following steps.[10,20] In our study, a Tafel plot of untreated Ag (overpotential versus log of the partial current density for CO production) in Figure 4b shows a Tafel slope of 133 mV/dec, which implies that the initial electron transfer for CO_2 activation is the RDS for the overall process (Scheme 1).[10,16] In contrast, a low Tafel slope of 60 mV/dec was obtained on AE-induced nanostructured Ag catalysts (4.9 μm) at relatively low overpotentials, indicating fast initial electron transfer to a CO_2 molecule for CO_2 activation (Scheme 1).[10,25] In addition, this low Tafel slope is consistent with a fast pre-equilibrium of the initial electron transfer prior to a RDS according to previous work.[25] Furthermore, a dramatically increased Tafel slope for nanostructured Ag was observed at relatively high overpotentials, implying that the electrocatalytic CO_2 reduction likely reaches a mass transport limitation.

It has been demonstrated that the initial proton donation is derived from HCO_3^-.[20,25] Thus, to further uncover the reaction mechanism (first proton donation step) on nanostructured Ag, the effect of HCO_3^- concentration on the CO_2 reduction activity was investigated. A plot of log(j_{co}) versus log-

DOI: 10.1021/acsenergylett.8b00472
ACS Energy Lett. 2018, 3, 1301−1306

Scheme 1. Proposed Reaction Paths for CO_2 Reduction to CO on Untreated Ag and Ag_2CO_3-Derived Nanostructured Ag[a]

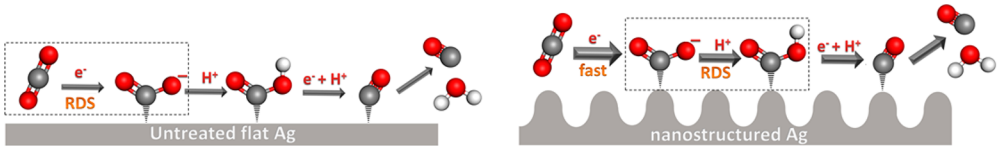

[a]The grey, red, and white balls represent C, O, and H atoms, respectively. Larger arrows indicate the relatively fast reaction steps.

($[HCO_3^-]$) in Figure 4c exhibits a slope of ~0.8, which corresponds to first-order dependence of the HCO_3^- concentration on the reaction rate, indicating that proton donation from HCO_3^- is a RDS for nanostructured Ag in the reduction of CO_2 to CO.[10,25] Thus, the RDS is switched from the first electron transfer for untreated Ag to the initial proton donation for nanostructured Ag (Scheme 1).

To better understand the charge transfer process at the electrode/electrolyte interface, electrochemical impedance spectroscopy (EIS) was performed at various potentials. The comparison of charge transfer resistance (R_{ct}) between untreated Ag and AE-Ag as a function of overpotential was extracted from EIS (Figure S9) based on the equivalent circuit (Figure 4d). As presented in Figure 4d, AE-Ag exhibited a much lower R_{ct} than that of polycrystalline Ag at identical conditions, suggesting a significantly accelerated charge transfer process on AE-Ag,[14] which may reflect the reduced activation energy barrier of electron transfer on nanostructured Ag. This result is consistent with fast initial electron transfer on nanostructured Ag according to Tafel analysis. In addition, a clear mass transport limitation for nanoporous Ag was observed at relatively high overpotentials in Nyquist plots (Figure S10), which is also in line with Tafel analysis (the dramatic increase in the Tafel slope at relatively high overpotentials). These results indicate that, while a mass transport limitation may be reached on nanoporous Ag at high overpotentials, the dramatically improved initial electron transfer for CO_2 activation enhances the intrinsic CO_2 reduction activity, resulting in high catalytic selectivity and activity for the electrocatalytic reduction of CO_2 to CO. EIS has seldom been used in CO_2 reduction experiments; thereby, the consistency between the Tafel analysis and EIS shows the potential for this technique to give meaningful information relating to mechanistic charge transfer processes for electrochemical CO_2 reduction.

In summary, a simple and fast anodic-etching procedure was used to fabricate highly active, selective, and stable Ag electrocatalysts for the reduction of CO_2 to CO. A high FE of >92% for CO was achieved on AE-Ag at a potential of −0.4 V vs RHE (overpotential of 290 mV). Notably, the AE-Ag was capable of maintaining a high catalytic selectivity of ~90% for CO production for >100 h, which remarkably outcompetes the currently reported durability of single-metal catalysts. The improved CO_2 reduction performance is attributed to the increased number of active sites for CO_2 reduction and the improved intrinsic CO_2 reduction activity by fast initial electron transfer. In this study, after prolonged CO_2 reduction, the procedure of anodic-etching can be performed subsequently on the same Ag electrocatalysts in the same $KHCO_3$ electrolyte that is used for CO_2 reduction to recover the robust catalytic performance. Thus, the Ag electrocatalysts, prepared by this fast, simple, and cost-effective approach, is capable of reducing CO_2 to CO with high catalytic selectivity and excellent stability, offering a very promising platform for industrial applications.

■ ASSOCIATED CONTENT

Supporting Information

The Supporting Information is available free of charge on the ACS Publications website at DOI: 10.1021/acsenergylett.8b00472.

Experimental details of Ag_2CO_3 fabrication, SEM, TEM, XRD, XPS, and CO_2 reduction measurement, thickness calculation of anodic-etched Ag, summarized tables of reported electrocatalysts, EASA measurement, calculation of j_{CO} and normalized j_{CO}, EIS, OH^- adsorption/desorption, *iR* correction, and error bars (PDF)

■ AUTHOR INFORMATION

Corresponding Authors

*E-mail: m.ma.cn@outlook.com (M.M.).
*E-mail: W.Smith@tudelft.nl (W.A.S.).

ORCID

Ming Ma: 0000-0003-3561-5710
Wilson A. Smith: 0000-0001-7757-5281

Notes

The authors declare no competing financial interest.

■ ACKNOWLEDGMENTS

This work is supported by an NWO VIDI grant awarded to W.A.S. The authors would like to thank Bartek J. Trześniewski for performing the XPS measurements. We also would like to thank Zerui Zhang for assistance in part of the proton transfer study experiments.

■ REFERENCES

(1) Whipple, D. T.; Kenis, P. J. A. Prospects of CO_2 utilization via direct heterogeneous electrochemical reduction. *J. Phys. Chem. Lett.* **2010**, *1*, 3451−3458.

(2) Kuhl, K. P.; Hatsukade, T.; Cave, E. R.; Abram, D. N.; Kibsgaard, J.; Jaramillo, T. F. Electrocatalytic conversion of carbon dioxide to methane and methanol on transition metal surfaces. *J. Am. Chem. Soc.* **2014**, *136*, 14107−14113.

(3) Qiao, J.; Liu, Y.; Hong, F.; Zhang, J. A review of catalysts for the electroreduction of carbon dioxide to produce low-carbon fuels. *Chem. Soc. Rev.* **2014**, *43*, 631−675.

(4) Ross, M. B.; Dinh, C. T.; Li, Y.; Kim, D.; De Luna, P.; Sargent, E. H.; Yang, P. Tunable Cu enrichment enables designer syngas electrosynthesis from CO_2. *J. Am. Chem. Soc.* **2017**, *139*, 9359−9363.

(5) Li, C. W.; Ciston, J.; Kanan, M. W. Electroreduction of carbon monoxide to liquid fuel on oxide-derived nanocrystalline copper. *Nature* **2014**, *508*, 504−507.

(6) Ma, M.; Djanashvili, K.; Smith, W. A. Controllable hydrocarbon formation from the electrochemical reduction of CO_2 over Cu nanowire arrays. *Angew. Chem., Int. Ed.* **2016**, *55*, 6680−6684.

(7) Li, C. W.; Kanan, M. W. CO_2 reduction at low overpotential on Cu electrodes resulting from the reduction of thick Cu_2O films. *J. Am. Chem. Soc.* **2012**, *134*, 7231−7234.

(8) Li, F.; Chen, L.; Knowles, G. P.; MacFarlane, D. R.; Zhang, J. Hierarchical mesoporous SnO_2 nanosheets on carbon cloth: a robust

DOI: 10.1021/acsenergylett.8b00472
ACS Energy Lett. 2018, 3, 1301−1306

and flexible electrocatalyst for CO_2 reduction with high efficiency and selectivity. *Angew. Chem., Int. Ed.* **2017**, *56*, 505−509.
(9) Hori, Y. Electrochemical CO_2 Reduction on Metal Electrodes. In *Modern Aspects of Electrochemistry*; Vayenas, C. G., White, R. E., Gamboa-Aldeco, M. E., Eds.; Springer, 2008; pp 89−189.
(10) Lu, Q.; Rosen, J.; Zhou, Y.; Hutchings, G. S.; Kimmel, Y. C.; Chen, J. G.; Jiao, F. A selective and efficient electrocatalyst for carbon dioxide reduction. *Nat. Commun.* **2014**, *5*, 3242.
(11) Hatsukade, T.; Kuhl, K. P.; Cave, E. R.; Abram, D. N.; Jaramillo, T. F. Insights into the electrocatalytic reduction of CO_2 on metallic silver surfaces. *Phys. Chem. Chem. Phys.* **2014**, *16*, 13814−13819.
(12) Lee, H.-E.; Yang, K. D.; Yoon, S. M.; Ahn, H.-Y.; Lee, Y. Y.; Chang, H.; Jeong, D. H.; Lee, Y.-S.; Kim, M. Y.; Nam, K. T. Concave rhombic dodecahedral Au nanocatalyst with multiple high-index facets for CO_2 reduction. *ACS Nano* **2015**, *9*, 8384−8393.
(13) Hall, A. S.; Yoon, Y.; Wuttig, A.; Surendranath, Y. Mesostructure-induced selectivity in CO_2 reduction catalysis. *J. Am. Chem. Soc.* **2015**, *137*, 14834−14837.
(14) Liu, M.; Pang, Y.; Zhang, B.; De Luna, P.; Voznyy, O.; Xu, J.; Zheng, X.; Dinh, C. T.; Fan, F.; Cao, C.; et al. Enhanced electrocatalytic CO_2 reduction via field-induced reagent concentration. *Nature* **2016**, *537*, 382−386.
(15) Asadi, M.; Kumar, B.; Behranginia, A.; Rosen, B. A.; Baskin, A.; Repnin, N.; Pisasale, D.; Phillips, P.; Zhu, W.; Haasch, R.; et al. Robust carbon dioxide reduction on molybdenum disulphide edges. *Nat. Commun.* **2014**, *5*, 4470.
(16) Kas, R.; Hummadi, K. K.; Kortlever, R.; De Wit, P.; Milbrat, A.; Luiten-Olieman, M. W. J.; Benes, N. E.; Koper, M. T. M.; Mul, G. Three-dimensional porous hollow fibre copper electrodes for efficient and high-rate electrochemical carbon dioxide reduction. *Nat. Commun.* **2016**, *7*, 10748.
(17) Vasileff, A.; Zheng, Y.; Qiao, S. Z. Carbon solving carbon's problems: recent progress of nanostructured carbon-based catalysts for the electrochemical reduction of CO_2. *Adv. Energy Mater.* **2017**, *7*, 1700759.
(18) Cui, X.; Pan, Z.; Zhang, L.; Peng, H.; Zheng, G. Selective etching of nitrogen-doped carbon by steam for enhanced electrochemical CO_2 reduction. *Adv. Energy Mater.* **2017**, *7*, 1701456.
(19) Kim, C.; Jeon, H. S.; Eom, T.; Jee, M. S.; Kim, H.; Friend, C. M.; Min, B. K.; Hwang, Y. J. Achieving selective and efficient electrocatalytic activity for CO_2 reduction using immobilized silver nanoparticles. *J. Am. Chem. Soc.* **2015**, *137*, 13844−13850.
(20) Rosen, J.; Hutchings, G. S.; Lu, Q.; Rivera, S.; Zhou, Y.; Vlachos, D. G.; Jiao, F. Mechanistic insights into the electrochemical reduction of CO_2 to CO on nanostructured Ag surfaces. *ACS Catal.* **2015**, *5*, 4293−4299.
(21) Qiu, J.; Tang, J.; Shen, J.; Wu, C.; Qian, M.; He, Z.; Chen, J.; Shuang, S. Preparation of a silver electrode with a three-dimensional surface and its performance in the electrochemical reduction of carbon dioxide. *Electrochim. Acta* **2016**, *203*, 99−108.
(22) Ma, M.; Trześniewski, B. J.; Xie, J.; Smith, W. A. Selective and efficient reduction of carbon dioxide to carbon monoxide on oxide-derived nanostructured silver electrocatalysts. *Angew. Chem., Int. Ed.* **2016**, *55*, 9748−9752.
(23) Yoon, Y.; Hall, A. S.; Surendranath, Y. Tuning of silver catalyst mesostructure promotes selective carbon dioxide conversion into fuels. *Angew. Chem., Int. Ed.* **2016**, *55*, 15282−15286.
(24) Vermaas, D. A.; Smith, W. A. Synergistic electrochemical CO_2 reduction and water oxidation with a bipolar membrane. *ACS Energy Lett.* **2016**, *1*, 1143−1148.
(25) Chen, Y.; Li, C. W.; Kanan, M. W. Aqueous CO_2 reduction at very low overpotential on oxide-derived Au nanoparticles. *J. Am. Chem. Soc.* **2012**, *134*, 19969−19972.
(26) Ma, M.; Djanashvili, K.; Smith, W. A. Selective electrochemical reduction of CO_2 to CO on CuO-derived Cu nanowires. *Phys. Chem. Chem. Phys.* **2015**, *17*, 20861−20867.
(27) Lu, Q.; Rosen, J.; Jiao, F. Nanostructured metallic electrocatalysts for carbon dioxide reduction. *ChemCatChem* **2015**, *7*, 38−47.
(28) Hsieh, Y.-C.; Senanayake, S. D.; Zhang, Y.; Xu, W.; Polyansky, D. E. Effect of chloride anions on the synthesis and enhanced catalytic activity of silver nanocoral electrodes for CO_2 electroreduction. *ACS Catal.* **2015**, *5*, 5349−5356.
(29) Dong, H.; Chen, G.; Sun, J.; Li, C.; Yu, Y.; Chen, D. A novel high-efficiency visible-light sensitive Ag_2CO_3 photocatalyst with universal photodegradation performances: Simple synthesis, reaction mechanism and first-principles study. *Appl. Catal., B* **2013**, *134*−*135*, 46−54.
(30) Murray, B. J.; Li, Q.; Newberg, J. T.; Menke, E. J.; Hemminger, J. C.; Penner, R. M. Shape- and size-selective electrochemical synthesis of dispersed silver(I) oxide colloids. *Nano Lett.* **2005**, *5*, 2319−2324.
(31) Yu, C.; Li, G.; Kumar, S.; Yang, K.; Jin, R. Phase transformation synthesis of novel Ag_2O/Ag_2CO_3 heterostructures with high visible light efficiency in photocatalytic degradation of pollutants. *Adv. Mater.* **2014**, *26*, 892−898.
(32) Chan, C.; Wu, J.; Li, J.; Cheung, Y. Polypropylene/calcium carbonate nanocomposites. *Polymer* **2002**, *43*, 2981−2992.
(33) Hoshi, N.; Kato, M.; Hori, Y. Electrochemical reduction of CO_2 on single crystal electrodes of silver Ag(111), Ag(100) and Ag(110). *J. Electroanal. Chem.* **1997**, *440*, 283−286.
(34) Blizanac, B. B.; Ross, P. N.; Marković, N. M. Oxygen reduction on silver low-index single-crystal surfaces in alkaline solution: rotating ring $disk_{Ag(hkl)}$ studies. *J. Phys. Chem. B* **2006**, *110*, 4735−4741.
(35) Jovic, B. M.; Jovic, V. D.; Stafford, G. R. Cyclic voltammetry on Ag(111) and Ag(100) faces in sodium hydroxide solutions. *Electrochem. Commun.* **1999**, *1*, 247−251.
(36) Horswell, S. L.; Pinheiro, A. L. N.; Savinova, E. R.; Danckwerts, M.; Pettinger, B.; Zei, M.-S.; Ertl, G. A comparative study of hydroxide adsorption on the (111), (110), and (100) faces of silver with cyclic voltammetry, ex situ electron diffraction, and in situ second harmonic generation. *Langmuir* **2004**, *20*, 10970−10981.
(37) Kortlever, R.; Shen, J.; Schouten, K. J. P.; Calle-Vallejo, F.; Koper, M. T. M. Catalysts and reaction pathways for the electrochemical reduction of carbon dioxide. *J. Phys. Chem. Lett.* **2015**, *6*, 4073−4082.
(38) Calle-Vallejo, F.; Koper, M. T. M. Theoretical considerations on the electroreduction of CO to C_2 species on Cu(100) electrodes. *Angew. Chem., Int. Ed.* **2013**, *52*, 7282−7285.
(39) Peterson, A. A.; Abild-Pedersen, F.; Studt, F.; Rossmeisl, J.; Nørskov, J. K. How copper catalyzes the electroreduction of carbon dioxide into hydrocarbon fuels. *Energy Environ. Sci.* **2010**, *3*, 1311.
(40) Hansen, H. A.; Varley, J. B.; Peterson, A. A.; Nørskov, J. K. Understanding trends in the electrocatalytic activity of metals and enzymes for CO_2 reduction to CO. *J. Phys. Chem. Lett.* **2013**, *4*, 388−392.

DOI: 10.1021/acsenergylett.8b00472
ACS Energy Lett. 2018, 3, 1301−1306